DispatchDate: 30.04.2019 · ProofNo: 370, p.1

nature materials

ARTICLES

https://doi.org/10.1038/s41563-019-0370-z

Long-range chiral exchange interaction in synthetic antiferromagnets

Dong-Soo Han[1,2,3,8], Kyujoon Lee[1,8], Jan-Philipp Hanke[1,4], Yuriy Mokrousov[1,4], Kyoung-Whan Kim[2], Woosuk Yoo[5], Youri Van Hees[3], Tae-Wan Kim[6], Reinoud Lavijsen[3], Chun-Yeol You[7], Henk J. M. Swagten[3], Myung-Hwa Jung[5*] and Mathias Kläui[1*]

The exchange interaction governs static and dynamic magnetism. This fundamental interaction comes in two flavours—symmetric and antisymmetric. The symmetric interaction leads to ferro- and antiferromagnetism, and the antisymmetric interaction has attracted significant interest owing to its major role in promoting topologically non-trivial spin textures that promise fast, energy-efficient devices. So far, the antisymmetric exchange interaction has been found to be rather short ranged and limited to a single magnetic layer. Here we report a long-range antisymmetric interlayer exchange interaction in perpendicularly magnetized synthetic antiferromagnets with parallel and antiparallel magnetization alignments. Asymmetric hysteresis loops under an in-plane field reveal a unidirectional and chiral nature of this interaction, which results in canted magnetic structures. We explain our results by considering spin–orbit coupling combined with reduced symmetry in multilayers. Our discovery of a long-range chiral interaction provides an additional handle to engineer magnetic structures and could enable three-dimensional topological structures.

Ferromagnets (FMs) and antiferromagnets (AFMs) possess collinear spin alignments within magnetic domains due to an interaction called the symmetric or Heisenberg exchange interaction. Although this conventional interaction is well-known, recently a different interaction moved into the forefront of interest, one that leads to non-collinear and chiral spin textures. This class of exchange interactions—antisymmetric exchange interaction or Dzyaloshinskii–Moriya interaction (DMI)[1–3]—stems from the spin–orbit coupled (SOC) electrons (or ions), which mediate the exchange interaction between neighbouring spins within a FM, and inversion symmetry breaking (ISB) that results in a finite amplitude of the net effect[3–5]. The antisymmetric component of different kinds of exchange interactions has been discovered in a variety of materials systems: examples include the antisymmetric terms of super-exchange and *s*–*d* exchange interactions in antiferromagnetic insulators[1,2] and metallic spin glasses[3], respectively. Very recently, the discovery of the intralayer DMI, which arises in systems with an ISB at interfaces between the FM and heavy metal layers[6] (Fig. 1a, left panel) and leads to an antisymmetric interaction between the magnetic moments within the ferromagnetic layer, has stimulated work in the field of spintronics[7–14]. In particular, it has opened fascinating new avenues for fundamental research[15], as well as highly efficient and fast spin-based information technologies[7,16–18].

Beyond this intralayer exchange interaction, there can also be an exchange interaction across ferromagnetic layers through an indirect interlayer exchange interaction (IEI), namely the Ruderman–Kittel–Kasuya–Yosida interaction. The IEI that couples the magnetic moments in two separate layers in a collinear fashion is a crucial element for many applications in modern magnetic storage devices and spin electronics as it enables synthetic AFMs, and recently attracted a renewed interest in the community in line with an emerging field of antiferromagnetic spintronics[17,19,20]. The studies on the IEI, however, have so far focused only on its symmetric part. However, from symmetry considerations, one expects that the IEI can also lead to the emergence of an antisymmetric IEI. Specifically, an antisymmetric IEI is possible in systems with ISB in the plane of thin films (Fig. 1a, right panel). An interesting feature of the antisymmetric IEI is that it leads to three-dimensional (3D) chiral magnetization configurations perpendicular to the film plane, in contrast to the antisymmetric component of the intralayer exchange interactions, which lead to chiral 2D spin structures confined only within individual magnetic layers. This opens the possibility to design 3D topological structures[21,22]. Despite its fundamental importance and the associated technological promises[17,19,21,23], clear experimental evidence of the antisymmetric IEI is conspicuously elusive[24,25].

In this article, we present an experimental demonstration of such a hitherto uncovered antisymmetric IEI in perpendicularly magnetized synthetic antiferromagnets (SAFs) with parallel and antiparallel magnetization alignments. We studied the multilayer reversal in different stacks and, using judiciously designed field sequences, we identified from unidirectional and chiral magnetization reversal the presence of an antisymmetric IEI and then examined this interaction with ab initio calculations.

We started by developing the necessary concepts to unambiguously identify the effect of antisymmetric IEI. In general, the magnetization reversal in FMs is invariant on the inversion of the magnetic field direction. However, this field-reversal invariance

[1]Institute of Physics, Johannes Gutenberg-Universität Mainz, Mainz, Germany. [2]Center for Spintronics, Korea Institute for Science and Technology, Seoul, Republic of Korea. [3]Department of Applied Physics, Institute for Photonic Integration, Eindhoven University of Technology, Eindhoven, The Netherlands. [4]Peter Grünberg Institut and Institute for Advanced Simulation, Forschungszentrum Jülich and JARA, Jülich, Germany. [5]Department of Physics, Sogang University, Seoul, Republic of Korea. [6]Department of Advanced Materials Engineering, Sejong University, Seoul, Republic of Korea. [7]Department of Emerging Materials Science, DGIST, Daegu, Republic of Korea. [8]These authors contributed equally: Dong-Soo Han and Kyujoon Lee. *e-mail: mhjung@sogang.ac.kr; klaeui@uni-mainz.de

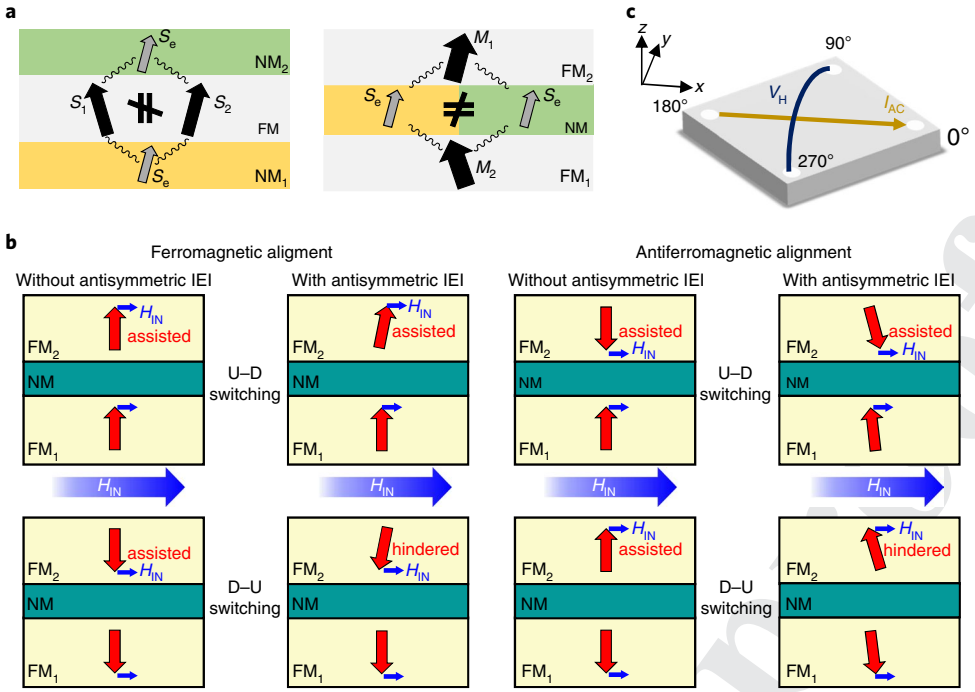

Fig. 1 | Antisymmetric IEI in synthetic AFMs. a, Schematic illustration of conduction electron-mediated exchange interactions between two atomic spins (left panel) and magnetic layers (right panel), which give rise to symmetric and antisymmetric intralayer exchange interactions and IEIs, respectively. The black arrows in the FMs represent either localized atomic spins ($S_{1,2}$) or magnetizations ($M_{1,2}$). The grey arrows show the spins of conduction electrons in non-magnetic (NM) layers. The green and yellow boxes in the left and right panels represent a broken inversion symmetry in the out-of-plane and in-plane directions of the films, respectively. The wavy lines represent mutual interaction between localized and itinerant spins. All the non-magnetic layers are assumed to include heavy elements with SOC. **b**, Schematics of symmetric and asymmetric switching of perpendicularly magnetized synthetic AFMs with parallel (left panel) and antiparallel (right panel) alignments of the layers due to a symmetric IEI and additionally in the presence and absence, respectively, of an antisymmetric IEI. The chirality of all the magnetization configurations displayed for 'with antisymmetric IEI' is right-handed. The red arrows indicate magnetizations of the top and bottom FMs. The blue arrows represent an in-plane bias field. H_{IN} breaks the inversion symmetry between U–D and D–U switching polarities only in the presence of antisymmetric IEI, due to the chiral magnetization alignments. **c**, Schematics of the experiments. The anomalous Hall effect is measured in the full sheet samples by using a van der Pauw method. The transverse Hall voltage (V_H) along the 90–270° line is measured as the a.c. current (I_{AC}) is applied parallel to the *x* axis that is along the 0–180° line.

does not hold if the inversion symmetry is broken in a given physical system. One particular example is the intralayer DMI[3]. In the presence of intralayer DMI, domain walls experience different effective fields according to their magnetic orderings, up-to-down (U–D) and down-to-up (D–U), under an in-plane magnetic field H_{IN} as the core magnetizations within domain walls of U–D and D–U align along opposite directions due to their preferred handedness by DMI. Consequently, when the domain wall moves, its dynamics becomes asymmetric with respect to H_{IN}, depending on the magnetic ordering[7,9,26,27].

Analogously, the antisymmetric IEI can break the field-reversal symmetry for the magnetization reversal. In the absence of the antisymmetric IEI, H_{IN} cannot break the inversion symmetry but only assist to lower the energy barrier for the magnetization reversal independent of the switching polarity (Fig. 1b). However, if the antisymmetric IEI is present, the chiral magnetization configurations are affected differently by H_{IN}, assisted or hindered in their magnetization switching depending on the sign of H_{IN} and the magnetization configurations. Particularly, they exhibit contrasting energy barriers for magnetization switching from parallel to antiparallel and antiparallel to parallel alignments as well as for the switching of D–U and U–D, as shown in the right panels of Fig. 1b (Supplementary Section 1). Accordingly, one would expect different switching fields with respect to the sweeping direction of the magnetic field, which would in turn result in the asymmetric magnetic hysteresis loops.

To test experimentally if the aforementioned asymmetric switching exists, which would indicate the presence of antisymmetric IEI, we measured the switching fields of typical SAFs of Ta(4)/Pt(4)/Co(0.6)/Pt(0.5)/Ru(t_{Ru})/Pt(0.5)/Co(1)/Pt(4) (layer thicknesses in nanometres) by sweeping the out-of-plane magnetic field, H_z, and simultaneously applied H_{IN} (Methods). Here two Co layers are coupled to each other via the symmetric IEI and perpendicularly magnetized with either parallel or antiparallel magnetization alignments at remanence. The magnetic hysteresis loops were measured by the anomalous Hall effect using the measurement configurations shown in Fig. 1c. For comparison, we also measured the switching fields of the reference sample Pt/Co/Pt/Ru that is nominally the same as the bottom half of the SAFs but without any IEI.

Figure 2a shows the magnetic hysteresis loops of Pt/Co/Pt/Ru and Pt/Co/Pt/Ru/Pt/Co/Pt with $t_{Ru}=0.4$ and 2.7 nm, respectively, for which the symmetric IEIs are ferromagnetic and antiferromagnetic and lead to parallel and antiparallel, respectively, alignment of the layers. Square hysteresis loops are clearly seen for all the structures, which shows that they have strong perpendicular magnetic anisotropy. Importantly, we found that the hysteresis loops for the SAFs with parallel and antiparallel coupling become significantly asymmetric when H_{IN} was applied, similar to the exchange bias effect. For the parallel coupling case, at $|\mu_0 H_{IN}|=100$ mT, a difference of approximately 0.7 mT in the switching fields ($\Delta\mu_0 H_{SW}$) between U–D and D–U was found. For the antiparallel coupling case, the hysteresis loop was seemingly biased to the left (right) at

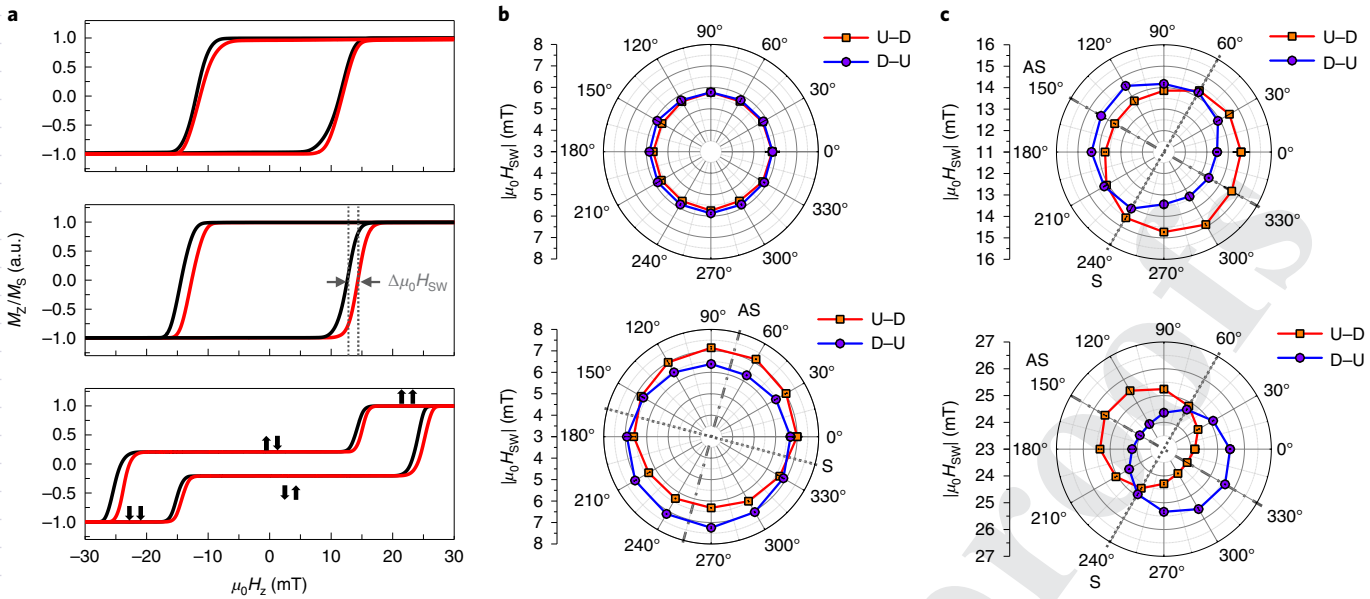

Fig. 2 | Chiral and unidirectional magnetization switching behaviours. a, Magnetic hysteresis loops measured by the anomalous Hall effect for the reference Pt/Co/Pt/Ru (top panel) and SAFs of Pt/Co/Pt/Ru/Pt/Co/Pt with parallel (middle panel) and antiparallel (bottom panel) coupling. The black and red curves indicate the hysteresis loops under the application of the negative and positive in-plane field of $|\mu_0 H_{IN}| = 100$ mT, respectively, which is applied along the asymmetric axis, as indicated in **b** and **c**. For Pt/Co/Pt/Ru/Pt/Co/Pt, the difference in switching fields, $\Delta\mu_0 H_{SW}$, under the application of $\mu_0 H_{IN} = \pm 100$ mT corresponds to ~0.7 mT. Four representative magnetization configurations for the antiparallel coupling case that appeared during the magnetization reversal are indicated by black arrows. **b**, Azimuthal angular dependence of the switching field of Pt/Co/Pt/Ru (top panel) and ferromagnetically coupled multilayers of Pt/Co/Pt/Ru/Pt/Co/Pt (bottom panel). The lines are to guide the eyes. **c**, Azimuthal angular dependence of the switching field of the top (top panel) and bottom (bottom panel) Co layers of antiferromagnetically coupled Pt/Co/Pt/Ru/Pt/Co/Pt. AS, asymmetric axis; S, symmetric axis; a.u., arbitrary units.

$\mu_0 H_{IN} = 100$ mT (-100 mT), which gave rise to $\Delta\mu_0 H_{SW} = 1.1$ and 1.4 mT for switching from parallel to antiparallel and from antiparallel to parallel alignments, respectively. Such asymmetric behaviour is in striking contrast to the results obtained from our reference sample of Pt/Co/Pt/Ru, in which the magnetic hysteresis loops are symmetric with respect to $H_z = 0$, irrespective of the sign of H_{IN}. The measured absence of inversion symmetry in the hysteresis loops is in obvious disagreement with the field-reversal symmetry, which demonstrates the presence of a symmetry-breaking interaction, such as antisymmetric IEI, in our SAFs. Moreover, we note that the field-reversal symmetry for Pt/Co/Pt/Ru in the same set-up also excluded any possible artefact from the misalignment of the in-plane magnet, which could otherwise cause an asymmetry in the hysteresis loop.

To understand the origin of the asymmetric switching behaviour, we next measured the azimuthal angular dependence of H_{SW}, as shown in Fig. 2b,c. The magnitude of the in-plane field was kept at $|\mu_0 H_{IN}| = 100$ mT as it rotated from 0 to 360°. In systems with inversion symmetry, one expects to see an isotropic or uniaxial (or multiaxial) anisotropy depending on the crystalline properties of the thin films, which was, indeed, found in our reference sample (Fig. 2b). Notably, however, we found that the magnetization switching for both SAFs with parallel and antiparallel alignment exhibited a unidirectional anisotropy for parallel (antiparallel) alignment with symmetric and asymmetric axes along the direction of H_{IN} // 75° (150°) and H_{IN} // 165° (240°), respectively (discussed in detail below). This highlights the unidirectional nature of the observed interlayer interaction. Interestingly, for the antiparallel coupling, we obtained markedly different unidirectional features in the two magnetic layers: for the case of the top Co layer (FM_{top}), the value of $|\mu_0 H_{SW}|$ for the U–D (D–U) was biased to 60° (240°), whereas for the bottom Co layer (FM_{bottom}), it was biased along the opposite direction. This opposite unidirectional behaviour between two magnetic layers unambiguously reveals that the observed unidirectional effect has a chiral nature (Supplementary Section 1) in line with an antisymmetric IEI. We note that the observed chiral behaviour is radically different from that expected from currently known magnetic interactions. For example, the biquadratic IEI is also responsible for non-collinear configurations[28], but leads to an isotropic behaviour without a preferred handedness, which is contrary to our observations, as seen in Fig. 2c. Furthermore, the current intralayer DMI cannot account for such asymmetric switching behaviour, because this interaction cannot produce the obtained asymmetric hysteresis unless it is combined with additional symmetry-breaking effects such as d.c. spin currents[26] or laterally asymmetric nanostructures[27] (Supplementary Section 2)[29,30].

The antisymmetric IEI is expected, in particular, to modify the dependence of H_{SW} on H_{IN}, which we plot in Fig. 3. For the structure with parallel coupling, the asymmetric behaviour between U–D and D–U switching is again clearly found for the case with H_{IN} is applied along the asymmetric axis, whereas almost symmetric behaviour is seen for H_{IN} parallel the symmetric axis (Fig. 3a,c). In particular, for the antiparallel coupling case, one can see that H_{IN} for local maxima (or minima) shifts away from $H_{IN} = 0$ mT for H_{IN} parallel to the antisymmetric axis, and the direction of the shift reverses for the opposite switching polarity (Fig. 3b). This shift of H_{SW} along the H_{IN} axis is a robust indicator for the presence of the antisymmetric IEI; the offset in the curves of H_{SW} versus H_{IN} indicates the presence of a built-in effective field, the sign and magnitude of which rely on the relative orientation of the magnetization between the top and bottom Co layers. This is analogous to the internal fields from the intralayer DMI, which depend on the magnetic ordering of domain wall structures[26]. However, this is in sharp contrast to the case without the antisymmetric IEI, where H_{IN} always assists in switching the

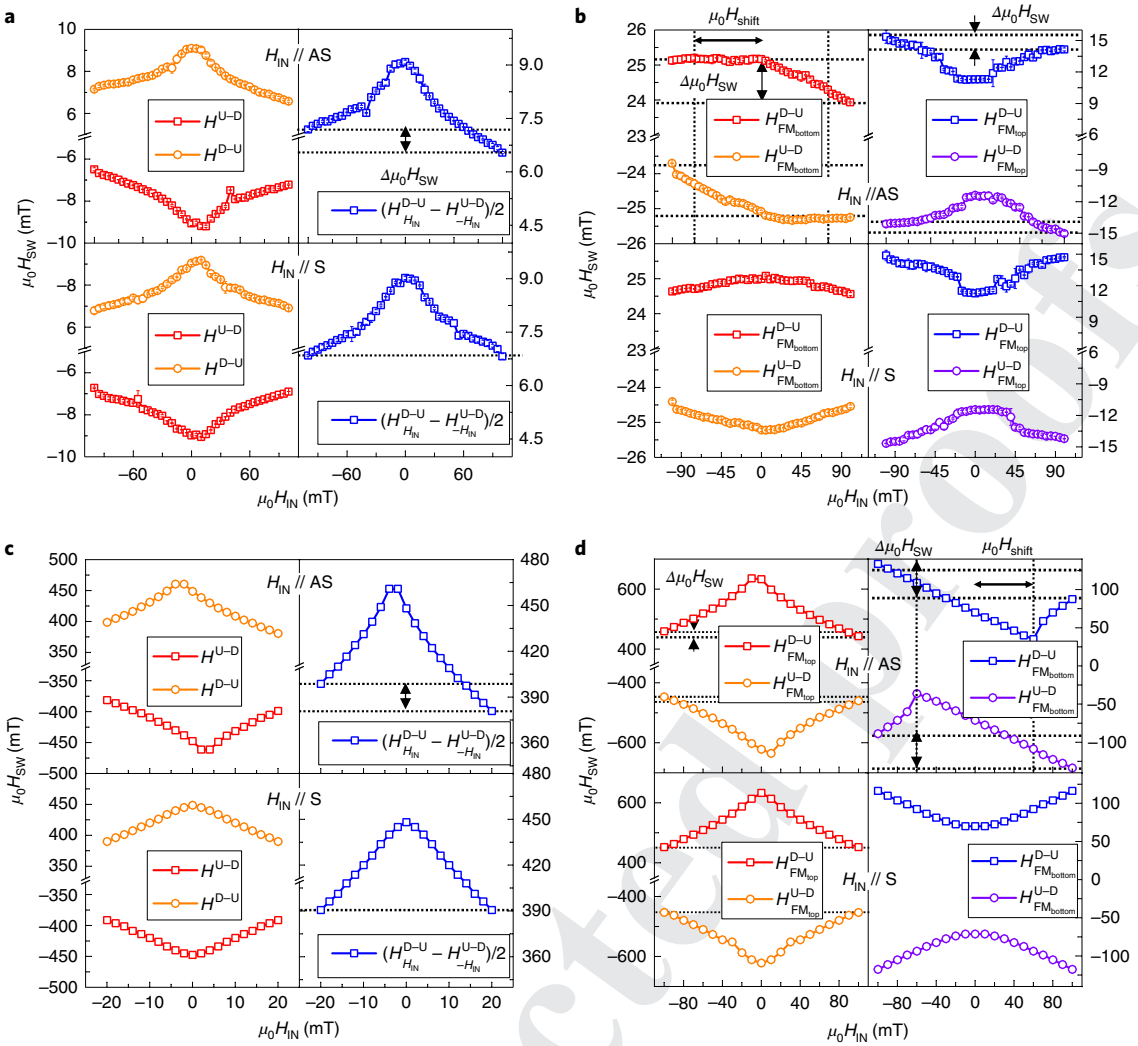

Fig. 3 | In-plane field dependence of magnetization switching fields. a, The experimentally measured H_{SW} as a function of H_{IN}, applied along asymmetric (top panel) and symmetric (bottom panel) axes as defined in Fig. 2, in SAFs with parallel coupling. The right panels in **a** represent the averaged $|H_{SW}|$ of U–D and D–U switching for H_{IN} and $-H_{IN}$. **b**, The experimentally measured switching field H_{SW} as a function of H_{IN} in SAFs with antiparallel coupling. The left (right) panels each represent the bottom (top) magnetic layers of the SAFs with antiparallel coupling. For both the parallel and antiparallel coupled cases, the symmetric (asymmetric) H_{SW} with respect to $H_{IN}=0$ is found when H_{IN} is applied along the symmetric (asymmetric) axis. **c**, Calculated H_{SW} as a function of H_{IN} for SAFs with parallel coupling by using a macrospin model (Methods). The right panels represent the averaged $|H_{SW}|$ of U–D and D–U switching for H_{IN} and $-H_{IN}$, respectively. **d**, Calculated H_{SW} as a function of H_{IN} for SAFs with antiparallel coupling. The left (right) panels each represent the top (bottom) magnetic layers of the SAFs with antiparallel coupling.

magnetization of perpendicularly magnetized materials irrespective of the sign of H_{IN} and switching polarity.

To validate the observed asymmetric switching behaviour by the antisymmetric IEI, we performed numerical calculations based on a macrospin model that incorporates the symmetric and antisymmetric IEI (details in Methods). The calculated azimuthal angular and field dependence of H_{SW} for the parallel and antiparallel couplings are presented in Fig. 3c,d, respectively. Although we reproduced the experimentally found asymmetric switching of the two layers, the order of the switching was found to be opposite for our numerical calculations, which is most probably due to thermal effects and imperfections in the experiment that are not incorporated into the calculations[31]. Taking into account the reversed switching sequence, however, we found that the numerical calculations are qualitatively in good agreement with the experimental data, and clearly reproduced the key signatures, which are the asymmetric and off-centred H_{SW} versus H_{IN}, as well as the unidirectional and chiral azimuthal angular dependence of H_{SW} (Supplementary Section 3), and these are the characteristic features that can only occur due to the presence of an antisymmetric IEI. From this we can conclude that the unidirectional switching behaviour results from the antisymmetric IEI present in our system.

To understand the microscopic origins of the necessary effective ISB in our polycrystalline samples, we next measured the spatially resolved magnetic hysteresis loops of the SAFs with the antiparallel coupling by using wide-field Kerr microscopy (Methods). In particular, we explored the minor hysteresis loops of the bottom layers (Fig. 4a inset) to explore the spatial distribution of the symmetric IEI without applying in-plane fields[32]. Interestingly, as shown in Fig. 4a, we found that the average of the two switching fields of the minor loops $H_z^{avg}=(H_1+H_2)/2$, which represents the strength of the symmetric IEI, has a unidirectional gradient. The axis of this gradient is parallel to the antisymmetric axis in Fig. 2c. This implies that the effective ISB, another key element for the antisymmetric IEI, results

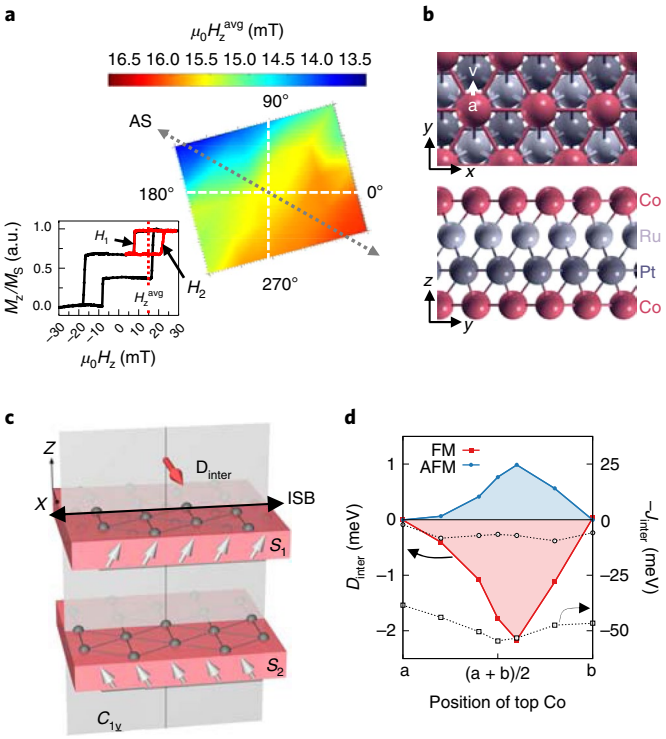

Fig. 4 | Effective symmetry breaking in sputtered samples and antisymmetric IEI from first principles. a, Spatial distribution of the symmetric IEI as obtained by polar Kerr microscopy. The inset represents magnetic hysteresis loops at a local area of the sample. The magnetic hysteresis loop was measured without applying an in-plane bias field. The red line indicates a minor loop of the bottom ferromagnetic layer. The H_z^{avg} was obtained from the average value of two switching fields in the minor loop. The line of 0–180° corresponds to the current line used for the anomalous Hall measurement. The symmetric and asymmetric axes correspond to the axis for which the symmetric and unidirectional behaviour, respectively, are the most prominent in Fig. 2. **b**, Top (top panel) and side (bottom panel) views of the thin Co/Ru/Pt/Co film. The high-symmetry locations a and b are marked, and the coloured arrow indicates the direction of the considered displacements of the top Co layer. **c**, Microscopic schematic of the chiral interlayer exchange in the C_{1y} structures. The collinear magnetization (grey arrows) of adjacent magnetic layers, represented as S_1 and S_2, acquires a relative canting due to the antisymmetric IEI as mediated by the $\mathbf{D}_{inter}$, which is perpendicular to the shaded mirror plane. The ISB is given along *y* axis. **d**, Effective symmetric and antisymmetric IEI constants $-J_{inter}$ (dotted lines) and D_{inter} (solid lines), respectively, as a function of the position of the top Co layer. The squares and circles refer to the cases of parallel and antiparallel coupling, respectively.

from the gradient in the symmetric IEI. Given that the symmetric IEI is most susceptible to the thickness of the non-magnetic spacers, we speculate that the effective symmetry breaking might be due to a thickness gradient, which can naturally appear during the sputtering. Particularly, our sputtered samples were grown without rotation of the sample holder during the growth, and therefore they are likely to lead to such an inhomogeneity, which gives rise to the thickness gradient along a certain axis.

Finally, to validate the observed antisymmetric IEI and uncover its minimal ingredients, we employed a theoretical ab initio method to scrutinize this interaction in magnetic heterostructures (Methods and Supplementary Section 4). We started with a Co/Ru/Pt/Co system with a collinear magnetization within each magnetic layer. Here we took into account the effective in-plane ISB by artificially adjusting the in-plane locations of the top Co from hollow sites a and b with C_{3v} symmetry into various positions with C_{1v} symmetry, as illustrated in Fig. 4b. One of the key manifestations of the antisymmetric IEI $D_{inter} \cdot (S_1 \times S_2)$ is a relativistic contribution to the total energy that is asymmetric with respect to the relative angle α between the magnetic moments S_1 and S_2 in the two Co layers. Indeed, our electronic structure calculations demonstrate such a unique signature of the antisymmetric IEI in the low-symmetric C_{1v} structures (Fig. 4c and Supplementary Fig. 7), which generally favours a non-zero canting between adjacent ferromagnetic layers due to the complex interplay with the conventional symmetric IEI. To assess the overall relevance of such a chiral interlayer interaction, we estimated for comparison the magnitude of the symmetric IEI $J_{inter}(S_1 \cdot S_2)$ by using an effective parameter J_{inter} that describes the small-angle region in the energy dispersion without SOC. Figure 4d presents the calculated values of both IEIs as a function of the position of the top magnet for an originally ferromagnetic or antiferromagnetic interaction between the ferromagnetic layers. Although the symmetric interaction exceeds the typical energy scale for the chiral IEI of 1.0 meV by one to two orders of magnitude in the studied system, the latter interaction is more susceptible to changes in the symmetry of the crystal lattice. In particular, the characteristic vector $\mathbf{D}_{inter}$ is required to be perpendicular to any mirror plane that connects interaction partners in the two layers (Fig. 4c), which renders the net antisymmetric IEI zero in C_{3v} systems but generally finite in the case of reduced symmetry. We point out that, although the microscopic origin of the ISB in our theoretical model is probably not reflecting the full ISB present in the experiment, our ab initio calculations clearly show that the presence of the antisymmetric IEI is enabled by any effective ISB. This then favours a chiral magnetization arrangement between separated magnetic layers, and thus demonstrates the crucial role of the in-plane ISB for the antisymmetric IEI. Any effective in-plane ISB, for example, from a thickness gradient or a lattice mismatch between different atomic layers, can give rise to the antisymmetric IEI. To corroborate this, we demonstrated that samples grown by an oblique sputtering technique that introduces tilted columnar microstructures[33,34] with a broken inversion symmetry also exhibit the unidirectional and chiral switching behaviour indicative of antisymmetric IEI. In particular, here the antisymmetric axis is exactly along the sputtering gradient axis. So our results demonstrate not only that, fundamentally, an ISB results in an antisymmetric IEI, but also that the effect can be engineered by tailoring and orienting a thickness gradient for a non-magnetic spacer layer[35] or introducing laterally asymmetric microstructures in a controlled fashion (Supplementary Section 5)[36].

So, overall, our combined experimental and theoretical work shows that we have completed the set of magnetic exchange interactions in systems with broken inversion symmetry: the antisymmetric IEI between two magnetic layers mediated by a non-magnetic spacer results from the ISB that can be tailored to eventually generate and control 3D magnetic textures. Specifically, we experimentally demonstrated the missing component of the IEI in SAFs with parallel and antiparallel alignments, which led to the asymmetric switching behaviours under in-plane bias fields. The observed asymmetric magnetization reversal is a unique signature of the chiral magnetization of the antisymmetric IEI. We identify the combination of SOC and the reduced in-plane symmetry as the microscopic origin of the observed antisymmetric IEI. Our findings not only uncover the antisymmetric component of the IEI in SAFs with parallel and antiparallel coupling, but also opens a path to investigate 3D topological spin structures by a chiral interlayer interaction that provides the tool for the implementation of 3D topological spin structures in future spintronic devices.

Online content

Any methods, additional references, Nature Research reporting summaries, source data, statements of code and data availability and

associated accession codes are available at https://doi.org/10.1038/s41563-019-0370-z.

Received: 1 December 2018; Accepted: 10 April 2019;

References

1. Dzyaloshinsky, I. A thermodynamic theory of 'weak' ferromagnetism of antiferromagnetics. *J. Phys. Chem. Solids* **4**, 241–255 (1958).
2. Moriya, T. Anisotropic superexchange interaction and weak ferromagnetism. *Phys. Rev.* **120**, 91–98 (1960).
3. Fert, A. & Levy, P. M. Role of anisotropic exchange interactions in determining the properties of spin-glasses. *Phys. Rev. Lett.* **44**, 1538–1541 (1980).
4. Kundu, A. & Zhang, S. Dzyaloshinskii–Moriya interaction mediated by spin-polarized band with Rashba spin–orbit coupling. *Phys. Rev. B* **92**, 94434 (2015).
5. Imamura, H., Bruno, P. & Utsumi, Y. Twisted exchange interaction between localized spins in presence of Rashba spin–orbit coupling. *AIP Conf. Proc.* **772**, 1409–1410 (2005).
6. Bode, M. et al. Chiral magnetic order at surfaces driven by inversion asymmetry. *Nature* **447**, 190–193 (2007).
7. Emori, S., Bauer, U., Ahn, S.-M., Martinez, E. & Beach, G. S. D. Current-driven dynamics of chiral ferromagnetic domain walls. *Nat. Mater.* **12**, 611–616 (2013).
8. Miron, I. M. et al. Fast current-induced domain-wall motion controlled by the Rashba effect. *Nat. Mater.* **10**, 419–423 (2011).
9. Ryu, K.-S., Thomas, L., Yang, S.-H. & Parkin, S. Chiral spin torque at magnetic domain walls. *Nat. Nanotechnol.* **8**, 527–533 (2013).
10. Mühlbauer, S. et al. Skyrmion lattice in a chiral magnet. *Science*. **323**, 915–919 (2009).
11. Yu, X. Z. et al. Skyrmion flow near room temperature in an ultralow current density. *Nat. Commun.* **3**, 988 (2012).
12. Woo, S. et al. Observation of room-temperature magnetic skyrmions and their current-driven dynamics in ultrathin metallic ferromagnets. *Nat. Mater.* **15**, 501–506 (2016).
13. Litzius, K. et al. Skyrmion Hall effect revealed by direct time-resolved X-ray microscopy. *Nat. Phys.* **13**, 170–175 (2016).
14. Moreau-Luchaire, C. et al. Additive interfacial chiral interaction in multilayers for stabilization of small individual skyrmions at room temperature. *Nat. Nanotechnol.* **11**, 444–448 (2016).
15. Kim, S. et al. Correlation of the Dzyaloshinskii–Moriya interaction with Heisenberg exchange and orbital asphericity. *Nat. Commun.* **9**, 1648 (2018).
16. Parkin, S. S. P., Hayashi, M. & Thomas, L. Magnetic domain-wall racetrack memory. *Science*. **320**, 190–194 (2008).
17. Yang, S.-H., Ryu, K.-S. & Parkin, S. Domain-wall velocities of up to 750 m s^{-1} driven by exchange-coupling torque in synthetic antiferromagnets. *Nat. Nanotechnol.* **10**, 221–226 (2015).
18. Kim, K.-J. et al. Fast domain wall motion in the vicinity of the angular momentum compensation temperature of ferrimagnets. *Nat. Mater.* **16**, 1187–1192 (2017).
19. Duine, R. A., Lee, K.-J., Parkin, S. S. P. & Stiles, M. D. Synthetic antiferromagnetic spintronics. *Nat. Phys.* **14**, 217–219 (2018).
20. Jungwirth, T. et al. The multiple directions of antiferromagnetic spintronics. *Nat. Phys.* **14**, 200–203 (2018).
21. Lavrijsen, R. et al. Magnetic ratchet for three-dimensional spintronic memory and logic. *Nature* **493**, 647–650 (2013).
22. Fernández-Pacheco, A. et al. Three-dimensional nanomagnetism. *Nat. Commun.* **8**, 15756 (2017).
23. Yang, Q. et al. Ionic liquid gating control of RKKY interaction in FeCoB/Ru/FeCoB and $(Pt/Co)_2/Ru/(Co/Pt)_2$ multilayers. *Nat. Commun.* **9**, 991 (2018).
24. Xia, K., Zhang, W., Lu, M. & Zhai, H. Noncollinear interlayer exchange coupling caused by interface spin-orbit interaction. *Phys. Rev. B* **55**, 12561–12565 (1997).
25. Vedmedenko, E. Y., Arregi, J. A., Riego, P. & Berger, A. Interlayer Dzyaloshinskii–Moriya interactions. Preprint at http://arXiv.org/cond-mat.mes-hall/:1803.10570 (2018).
26. Je, S. G. et al. Asymmetric magnetic domain-wall motion by the Dzyaloshinskii–Moriya interaction. *Phys. Rev. B* **88**, 214401 (2013).
27. Lo Conte, R. et al. Role of B diffusion in the interfacial Dzyaloshinskii–Moriya interaction in $Ta/Co_{20}Fe_{60}B_{20}/MgO$ nanowires. *Phys. Rev. B* **91**, 14433 (2015).
28. Demokritov, S. O. Biquadratic interlayer coupling in layered magnetic systems. *J. Phys. D* **31**, 925 (1998).
29. Pai, C.-F., Mann, M., Tan, A. J. & Beach, G. S. D. Determination of spin torque efficiencies in heterostructures with perpendicular magnetic anisotropy. *Phys. Rev. B* **93**, 144409 (2016).
30. Han, D. S. et al. Asymmetric hysteresis for probing Dzyaloshinskii–Moriya interaction. *Nano Lett.* **16**, 4438–4446 (2016).
31. Koplak, O. et al. Magnetization switching diagram of a perpendicular synthetic ferrimagnet CoFeB/Ta/CoFeB bilayer. *J. Magn. Magn. Mater.* **433**, 91–97 (2017).
32. Lavrijsen, R. et al. Tuning the interlayer exchange coupling between single perpendicularly magnetized CoFeB layers. *Appl. Phys. Lett.* **100**, 52411 (2012).
33. Barranco, A., Borras, A., Gonzalez-Elipe, A. R. & Palmero, A. Perspectives on oblique angle deposition of thin films: from fundamentals to devices. *Prog. Mater. Sci.* **76**, 59–153 (2016).
34. Alvarez, R. et al. Nanostructured Ti thin films by magnetron sputtering at oblique angles. *J. Phys. D* **49**, 045303 (2016).
35. Yu, G. et al. Switching of perpendicular magnetization by spin–orbit torques in the absence of external magnetic fields. *Nat. Nanotechnol.* **9**, 548–554 (2014).
36. Ummelen, F. C., Swagten, H. J. M. & Fernández-Pacheco, A. *Canted States in Anti-ferromagnetically Coupled Magnetic Bilayers*. Master thesis, Technische Universiteit Eindhoven (2013).
37. Kurz, P., Förster, F., Nordström, L., Bihlmayer, G. & Blügel, S. Ab initio treatment of noncollinear magnets with the full-potential linearized augmented plane wave method. *Phys. Rev. B* **69**, 24415 (2004).

Acknowledgements

We acknowledge insightful discussions with M. Hoffmann, S. Blügel, B. Dupé and S.-B. Choe. We acknowledge F. Ummelen for personal discussions on her results that are relevant to this work[37]. D.-S.H., K.L. and M.K. acknowledge support from MaHoJeRo (DAAD Spintronics network, project number 57334897) and the German Research Foundation (in particular SFB TRR 173 Spin+X). K.L. acknowledges the European Union's Horizon 2020 research and innovation programme under the Marie Skłodowska-Curie grant agreement Standard EF no. 709151. M.-H.J. acknowledges support from the National Research Foundation (NRF) of Korea grant funded by the Korea government (MEST) (nos 2017R1A2B3007918 and 2016M3A7B4910400). C.-Y.Y. acknowledges support from the NRF of South Korea under Grant 2017R1A2B3002621, and J.-P.H. and Y.M. acknowledge computing time on the supercomputers JUQUEEN and JURECA at the Jülich Super-computing Center, and at the JARA-HPC cluster of RWTH Aachen, as well as funding under the SPP 2137 "Skyrmionics" (project MO 1731/7-1) and project MO 1731/5-1 of the Deutsche Forschungsgemeinschaft (DFG). D.-S.H. and K.-W.K. were supported by the Korea Institute of Science and Technology (KIST) institutional program (no. 2E29410) and a National Research Council of Science & Technology (NST) grant (no. CAP-16-01-KIST) funded by the Korea government (Ministry of Science and ICT). K.-W.K. acknowledges the DFG (no. SI 1720/2-1).

Author contributions

M.-H.J. and D.-S.H. conceived the original idea. D.-S.H., K.L., M.-H.J. and M.K. planned and designed the experiments. D.-S.H. and Y.V.H. fabricated the samples with R.L. and H.J.M.S. D.-S.H. and K.L. performed transport measurements with W.Y. and data analysis under the supervision of M.K. and M.-H.J. T.-W.K. provided $[Pt/CoSiB]_2$/Pt multilayers. J.-P.H. and Y.M. performed the first-principles calculations and the analysis of relevant data. K.-W.K. provided theoretical explanations in Supplementary Information. D.-S.H. and C.-Y.Y. performed the numerical calculation based on a macrospin model. D.-S.H. wrote the paper with K.L., J.H. and M.K. All the authors discussed the results and commented on the manuscript.

Competing interests

The authors declare no competing interests.

Additional information

Supplementary information is available for this paper at https://doi.org/10.1038/s41563-019-0370-z.

Reprints and permissions information is available at www.nature.com/reprints.

Correspondence and requests for materials should be addressed to M.-H.J. or M.K.

Publisher's note: Springer Nature remains neutral with regard to jurisdictional claims in published maps and institutional affiliations.

Methods

Sample preparation and anomalous Hall measurement. The magnetic multilayers were grown on a silicon wafer coated with a 100 nm thick SiO_2 by using a ultrahigh vacuum magnetron d.c. sputtering system at a base pressure of 9.5×10^{-8} mbar and a working pressure of 2×10^{-2} mbar. Multilayers of Si/Ta(4)/Pt/(4)/Co(1.0)/Pt(0.7)/Ru(t_{Ru})/Pt(0.7)/Co(0.9)/Pt(4) were grown at room temperature. The Ru is used for the spacer, which provides a strong IEI, and the Pt layers between the top and bottom Co layers are used to enhance the perpendicular magnetic anisotropy of both ferromagnetic layers. To investigate the Ru-thickness dependent interlayer interaction, a wedge-shaped sample of Ta/Pt/Co/Pt/Ru/Pt/Co/Pt, in which the Ru thickness was varied from 0 to 4 nm, was preliminarily grown, and the oscillatory behaviour of magnetic hysteresis loops was measured by the magneto-optical Kerr effect in a polar configuration. The Ru thicknesses used in article and Supplementary Information were selected from the result. The hysteresis loops of the magnetic multilayers were measured by the anomalous Hall signal on an approximately 5×5 mm^2 sized continuous film by using a Van der Pauw method while sweeping the magnetic field in the out-of-plane and simultaneously applying a constant in-plane magnetic field. For the transport measurement, a sinusoidal current with a frequency of 13.7 Hz and a peak-to-peak amplitude of ~1 mA was used as a current source, and a lock-in technique was used to detect the Hall signal. The spatially resolved magnetic hysteresis loops were measured by using a wide-field Kerr microscope in a polar configuration. Q11 The magnetic hysteresis loops at 30 different positions within an approximately 5×5 mm^2 sized continuous film sample of Pt/Co/Pt/Ru/Pt/Co/Pt with antiparallel coupling were measured. The field of view of each area corresponds to $\sim1\times1$ mm^2. The hysteresis loops are measured by sweeping out-of-plane fields with no in-plane fields applied. Thus, for all the regions, magnetic hysteresis loops symmetric with respect to the out-of-plane field were observed.

Macrospin modelling. To explore the effect of the antisymmetric IEI and other magnetic interactions on the magnetization reversal, we employed a macrospin model that finds an equilibrium magnetization configuration through minimization of the total free energy functional. The total free energy functional consists of anisotropic energy, Zeeman energy and symmetric and antisymmetric exchange energies, and is given by: Q12

$$E_{tot} = -\mu_0 M_{S,top} t_{top} \mathbf{m}_{top} \cdot B - \mu_0 M_{S,bottom} t_{bottom} \mathbf{m}_{bottom} \cdot B$$
$$-K_{top} t_{top} (\mathbf{m}_{top} \cdot \hat{\mathbf{z}})^2 - K_{bottom} t_{bottom} (\mathbf{m}_{bottom} \cdot \hat{\mathbf{z}})^2$$
$$-J_{inter} \mathbf{m}_{top} \cdot \mathbf{m}_{bottom} - \mathbf{D}_{inter} \cdot (\mathbf{m}_{top} \times \mathbf{m}_{bottom})$$

Here, M_s is the saturation magnetization, $\mathbf{m}$ the magnetization vector, K the effective anisotropy constant, μ_0 the vacuum permeability, B the external magnetic field, t the thickness of a magnetic layer, $\hat{z}$ the unit vector normal to the surface, J_{inter} the coefficient for symmetric IEI and $\mathbf{D}_{inter}$ the DMI vector for antisymmetric IEI. The subscripts 'top' and 'bottom' describe the top and bottom magnetic layers, respectively. For a model system of Pt/Co/Pt/Ru/Pt/Co/Pt, we used the following material parameters: $M_s = 1.1\times10^6$ A m^{-1}, and $K = 2.24\times10^5$ and 5.25×10^5 J m^{-3} for the bottom and top layers, respectively. The coefficients for the symmetric IEI $J_{inter} = 2.1\times10^{-4}$ and -2.0×10^{-4} mJ m^{-2} and the antisymmetric IEI D_{inter}, which correspond to $|D_{inter}/J_{inter}| = 0.1$ and 0.03, respectively, were used for the SAFs with the parallel and antiparallel coupling, respectively.

First-principles calculations. Using material-specific density functional theory as implemented in the full-potential linearized augmented-plane-wave code FLEUR (www.flapw.de), we studied the electronic structure of a thin Co/Ru/Pt/Co film in a supercell geometry. The lattice constant of the in-plane hexagonal lattice was $5.211a_0$ (where a_0 is Bohr's radius), the distance between the two Co layers was $12.765a_0$ and we assumed a face-centred cubic stacking but variable in-plane positions of the top magnetic layer. Based on the generalized gradient approximation[38], the self-consistent calculations of the system without SOC were performed using a plane-wave cutoff of $4.0a_0^{-1}$ and the full Brillouin zone was sampled by 1,024 points. By including the effect of SOC to the first order, we unambiguously determined the magnitude of the antisymmetric IEI from the change in the energy dispersion of that coned spin spirals[39] that propagated perpendicular to the film. In these force-theorem calculations with SOC, the Brillouin zone was sampled by 4,096 points. Choosing a large enough distance between different super cells, we explicitly ensured that periodic images of the slab did not contribute to the obtained magnetic interaction parameters.

Data availability

The data sets generated during and/or analysed during the current study are available from the corresponding author on reasonable request.

References

38. Perdew, J. P., Burke, K. & Ernzerhof, M. Generalized gradient approximation made simple. *Phys. Rev. Lett.* **77**, 3865–3868 (1996).
39. Schweflinghaus, B., Zimmermann, B., Heide, M., Bihlmayer, G. & Blügel, S. Role of Dzyaloshinskii–Moriya interaction for magnetism in transition-metal chains at Pt step edges. *Phys. Rev. B* **94**, 24403 (2016).